Modelling yarn balloon motion in ring spinning

Zheng-Xue Tang [a,*], W. Barrie Fraser [b] and Xungai Wang [a]

[a] *School of Engineering and Technology, Deakin University, Geelong, VIC 3217, Australia*

[b] *School of Mathematics and Statistics, the University of Sydney, Sydney, NSW 2006, Australia*

Abstract

Air-drag on a ballooning yarn and balloon shape affect the yarn tension and ends-down (yarn breakage), which in turn affects energy consumption and yarn productivity in ring spinning. In this article, a mathematical model of yarn ballooning motion in ring spinning is established. The model can be used to generate balloon shape and predict tension in the ballooning yarn under given spinning conditions. Yarn tension was measured using a computer data acquisition system and the balloon shapes were captured using a digital camera with video capability during the experiments using cotton and wool yarns at various balloon-heights and with varying yarn-length in the balloon. The air-drag coefficients on ballooning cotton and wool yarns in ring spinning were estimated by making a "best fit" between the theoretical and experimental turning points. The theoretical results were verified with experimental data. The effects of air-drag and balloon shape on yarn tension are discussed.

Keywords: Ring spinning; Ballooning yarn; Yarn tension; Air-drag

[*] Corresponding author – *Email address*: ztang@deakin.edu.au.

1 Introduction

Ring spinning is the dominant system of manufacturing high quality yarns from staple fibres for apparel applications. The principle of ring spinning is depicted in Fig. 1. A bundle of parallel fibres (the roving) is fed to the drafting zone. The difference in surface velocity of the front (faster) and back (slower) drafting rollers will attenuate the roving to a thinner strand of parallel fibres, under the control of the double aprons. The thin strand of parallel fibres emerging from the front rollers is then simultaneously twisted and wound onto a yarn package (i.e., cop) mounted on a driven spindle. The twisted thin strand of fibres, now called a yarn, is threaded through a traveller and a yarn guide and balloons out between these two elements during normal spinning. The twisted yarn is then wound onto the bobbin or yarn package.

Because of the careful fibre control during the spinning process, ring spinning produces relatively high quality yarns and the quality of ring spun yarns has been used as a benchmark against which the quality of yarns produced on other spinning systems is judged [1]. However, the energy consumption for overcoming yarn wind-on tension, which is proportional to the tension in balloon in ring spinning [2], is much higher than that in other spinning systems. The air-drag on a ballooning yarn increases the yarn tension and affects balloon shape. Therefore, controlling the air-drag on a ballooning yarn and reducing the tension in ballooning yarn will decrease energy consumption and increase productivity in ring spinning mills.

Many researchers have studied the dynamics of ballooning yarns in ring spinning. Bracewell and Greenhalgh [3] investigated tension in spinning balloon and relationships between the

yarn tension and the tension at the guide-eye with a dynamical analysis based on the assumption that the spinning balloon has a single loop. De Barr [4–6] described the relationship between spinning tension and balloon shape and air-drag in ring spinning. Batra *et al*. [7, 8] analysed the dynamics of ring spinning process with an integrated approach. Fraser's [9–13] recent studies of tension and corresponding balloon shapes showed that the equations admitted multiple solutions typical of nonlinear systems exhibiting the bifurcation phenomenon under certain operating conditions. He also investigated the characteristics of air-drag on the ring spinning balloon, such as the effects of air-drag magnitude on balloon shape, and tension and the bifurcation behaviours of the solution. The experimental work which was used to confirm the theoretical predictions can be found in the literature. Zhu *et al*. [14, 15] measured tension at upper-eyelet using rubber string and filament polyester yarn on a Balloon Test System (BTS). Sharma and Rahn [16] measured eyelet tension using continuous-filament polyester-fibre yarn on BTS with a control ring. Also Clark *et al*. [13] sketched an experimental yarn balloon apparatus (as shown in Fig. 2) and carried out the experiments using a particular yarn. However, there is lack of experiments on the common cotton and wool yarns spun at varying balloon-heights.

This paper extends the cited prior research by studying natural yarn and proposes a method of estimating the air-drag coefficient used in the theoretical model and predicting the tension in ballooning cotton and wool yarns for yarn manufacturers. After establishing the mathematical model of yarn balloon motion in ring spinning, a program corresponding to the model is developed using MATLAB software. The experiments simulating yarn winding in ring spinning are described. Based on the comparisons of theoretical and experimental curves of guide-eye tension against yarn-length in the balloon, the air-drag coefficients on the ballooning cotton and wool yarns were estimated. From the resulting theoretical and

experimental balloon shapes, the relationship between yarn tension and balloon loops was analysed. The effects of air-drag, rotational speed, balloon loop and balloon-height on yarn tension are discussed.

2 Theoretical model

2.1 Mathematical formulation

We consider a yarn balloon that rotates at a constant angular velocity ω [radian per second] (clockwise rotation, from top down) during ring spinning, as shown in Fig. 3. Let $\boldsymbol{e}_r$, $\boldsymbol{e}_\theta$, $\boldsymbol{k}$ be unit based vectors of a cylindrical coordinate system so that a material point $\boldsymbol{P}$ on a rotating yarn has coordinate (r, θ, z). The height and ring radius of the yarn balloon are h [m] and a [m], respectively. The distance measured along the yarn from the guide-eye $\boldsymbol{O}$ to the point $\boldsymbol{P}$ is s [m]. If the balloon shapes are considered to be stationary when viewed from the rotating reference frame, the position vector of $\boldsymbol{P}$ can be expressed as $\boldsymbol{R}(s) = r\boldsymbol{e}_r + z\boldsymbol{k}$.

The yarn is assumed to have the following properties: (i) the yarn is perfectly flexible, (ii) the yarn is inextensible, (iii) the effect of yarn twist is ignored, and (iv) the linear density of the yarn is uniform. Following the work of Fraser [9], the *vector form* of the stationary-balloon *{in which the yarn path is stationary relative to the rotating frame}* system for the yarn element at $\boldsymbol{P}$ can be written as

$$m\left\{\omega^2\boldsymbol{k}\times(\boldsymbol{k}\times\boldsymbol{R})\right\} = \left(T\boldsymbol{R}'\right)' + \boldsymbol{F} \qquad (1a)$$

$$\boldsymbol{R}'\bullet\boldsymbol{R}' = 1 \qquad (1b)$$

$$\boldsymbol{F} = -\frac{1}{2}\rho d C_D|\boldsymbol{v}_n|\boldsymbol{v}_n \qquad (1c)$$

with boundary conditions

$$\boldsymbol{R}(0) = \mathbf{0} \tag{1d}$$

$$\boldsymbol{R}(s_l) = a\,\boldsymbol{e}_r + h\boldsymbol{k} \tag{1e}$$

where m [kg/m] is the linear density of the yarn, $T(s)$ [N] is the tension in the yarn at $\boldsymbol{P}$, $(\,)' \equiv d(\,)/ds$, ρ [kg/m^3] is air density, d [m] is yarn diameter in balloon, C_D [scalar] is air-drag coefficient on the ballooning yarn, s_l [m] is yarn-length in balloon, and $\boldsymbol{v}_n$ is the normal component of the yarn velocity at point $\boldsymbol{P}$.

We now introduce the dimensionless variables: $\bar{\boldsymbol{R}} = \dfrac{\boldsymbol{R}}{a} = \dfrac{r}{a}\boldsymbol{e}_r + \dfrac{z}{a}\boldsymbol{k} = \bar{r}\,\boldsymbol{e}_r + \bar{z}\,\boldsymbol{k}$, $\bar{s} = \dfrac{s}{a}$, $\bar{\boldsymbol{v}}_n = \dfrac{\boldsymbol{v}_n}{\omega a}$, $\bar{\boldsymbol{v}} = \dfrac{\boldsymbol{v}}{\omega a}$, $\bar{h} = \dfrac{h}{a}$, $\bar{T} = \dfrac{T}{m\omega^2 a^2}$, $\bar{\boldsymbol{F}} = \dfrac{\boldsymbol{F}}{m\omega^2 a}$ and $p_0 = \dfrac{8a\rho d C_D}{m}$. The system (1) has the *normalized form* as follows:

$$\boldsymbol{k}\times(\boldsymbol{k}\times\boldsymbol{R}) = (T\boldsymbol{R}')' - \frac{1}{16}p_0|\boldsymbol{v}_n|\boldsymbol{v}_n \tag{2a}$$

$$\boldsymbol{v}_n = \boldsymbol{R}'\times((\boldsymbol{k}\times\boldsymbol{R})\times\boldsymbol{R}') \tag{2b}$$

$$\boldsymbol{R}'\bullet\boldsymbol{R}' = 1 \tag{2c}$$

with boundary conditions

$$\boldsymbol{R}(0) = \mathbf{0} \tag{2d}$$

$$\boldsymbol{R}(s_l) = \boldsymbol{e}_r + h\boldsymbol{k}. \tag{2e}$$

The cylindrical coordinate components of these equations are:

$$-r = T'r' + Tr'' - Tr\theta'^2 + \frac{1}{16}r^3 r'\,\theta'\,p_0\sqrt{r'^2+z'^2} \tag{3a}$$

$$0 = T'r\theta' + 2Tr'\,\theta' + Tr\theta'' - \frac{1}{16}r^2 p_0\left(\sqrt{r'^2+z'^2}\right)^3 \tag{3b}$$

$$0 = T'z' + Tz'' + \frac{1}{16} r^3 \theta' z' \; p_0 \sqrt{r'^2 + z'^2} \qquad (3c)$$

where $0 \le s \le s_l$, $(\;)' \equiv d(\;)/ds$, the normal speed is $r\sqrt{r'^2 + z'^2}$. On forming the scalar product of Equation (2*a*) with $\boldsymbol{R}'(s)$ using inextensibility condition (2*c*) and integrating the resultant equation, we find the tension equation

$$T = T_0 - \frac{1}{2} r^2 \qquad (3d)$$

in which T_0 is the tension at guide-eye and r is the balloon radius at $\boldsymbol{P}$. The boundary conditions become

$$r(0) = 0,\ \theta(0) = 0,\ z(0) = 0,\ \theta'(0) = 0,\ z'(0) = \sqrt{1 - r'^2(0)}\ ,\ r(s_l) = 1,\ z(s_l) = h \qquad (3e)$$

2.2 Program development

Equations (3) are the components of the normalized form in a cylindrical coordinate system. They are equivalent to a system of seven first-order ordinary differential equations. The problem is now reduced to a two-point boundary-value problem for ODEs which can be solved by a shooting method [17]. We implemented a program on this problem using MATLAB language [18]. A Runge-Kutta ODE solver is used to integrate the component equations. For a given value $\varepsilon > 0$, a modification of the Powell minimization method is then used to iterate the trial values until the approximate error

$$E = |r(s)\big|_{s=s_l} - 1| + |z(s)\big|_{s=s_l} - h| < \varepsilon \qquad (4)$$

2.3 Examples from simulation

On a PC (Intel ® Pentium ® 4, CUP 2.53 GHz AT/AT compatible, 1 GB RAM) with Operation System Windows 2000 (professional version) and the software MATLAB, we simulated the tension at guide-eye against yarn-length in balloon and the balloon shape for various normalized air-drag coefficient (p_0) on the ballooning yarn using the previous developed program because p_0 is unique parameter in the system (3).

2.3a The tension at guide-eye against yarn-length in balloon

We simulated the tension at guide-eye against the yarn-length in balloon ($\overline{s_l}$) ($10.3 \le \overline{s_l} \le 13.5$) at a balloon-height of 10 for varying values of p_0 from 1 to 30. The results show that:

(1) The larger the value of p_0, the more rapid is the decrease of guide-eye tension as the yarn-length in the balloon is increased;

(2) For any given yarn-length in balloon, the tension at the guide-eye corresponding to the smaller value of p_0 is not less than the tension at the guide-eye corresponding to the larger value of p_0;

(3) when $p_0 \ge 7$, the tension at guide-eye decreases when yarn-length in balloon is increased;

(4) The larger the value of p_0, the fewer the time to be taken for simulation.

Fig. 4 displays the partial curves of tension at guide-eye against yarn-length in balloon from the simulations.

2.3b The balloon shapes with varying yarn-length in balloon

We used the previous program to generate balloon shape at balloon-height of 10 and $p_0 = 3.3$ and with varying yarn-length in balloon. Table 1 displays the partial simulated data, which show that, when $s_l > 10.05$, the approximate error

$$E = |r(s)\big|_{s=s_l} - 1| + |z(s)\big|_{s=s_l} - h| < 0.024.$$

The results also show that, while yarn-length in the balloon is increased, the yarn tension at guide-eye decreases but the offset-angle (i.e., the lag angle of a ballooning yarn at the rotating eyelet relative to the plane containing the axis of rotation and the yarn tangent vector at the guide-eye, see φ in Fig. 5) in balloon increases. This is consistent with our previous experimental results [19].

3 Experimental setup

A ballooning rig, as shown in Fig. 6, was used to measure the yarn tension at the guide-eye [19]. It consists of a motor controller attached to the yarn ballooning device, a computer data acquisition system, and Instron testing machine with a separate tension sensor mounted on its crosshead through an arm. The “ring radius” or distance between the rotating eyelet and the centre of the ballooning device is fixed at 30 mm. The vertical distance between the guide-eye and the eyelet is the balloon-height and can be pre-set by adjusting the guide-eye position. The guide-eye is vertically aligned with the centre of the yarn ballooning device.

One end of the yarn, which passes through the guide-eye, is attached to the tension sensor and the other end is fixed to the eyelet. The yarn segment between the guide-eye and eyelet forms a ballooning curve while the eyelet is rotating and this segment is defined as the yarn-length in the balloon. The yarn-length in the balloon increases as the arm, on which the tension sensor is fixed, moves downward. When the arm goes to its lower limit, the yarn-length in balloon reaches the “maximum” value. The yarn-length in the balloon decreases as the arm moves upward until it reaches the upper limit. The arm speed is pre-set at 200 mm/min. When the eyelet starts rotating, the yarn segment between the guide-eye and rotating eyelet generate yarn tension and the tension signal at the guide-eye is digitised by the computer data acquisition system.

We used three different types of yarns with various counts for the experiments. For yarn tension measurement, we ‘spun’ the yarns at different rotational speeds on the ballooning rig with the balloon-height varying from 120 mm to 360 mm. We measured the yarn rotational speed with a digital tachometer during the tests, and used a digital camera with video capability to capture the balloon shape.

Fig. 7 shows the normalized experimental curves of tension at guide-eye against yarn-length in balloon for various yarns, where data have been converted into normalized form using the relationships mentioned in section 2.1.

4 Results and Discussion

The theoretical model in this study is based on the simplifying assumption that the balloon rotates in still air so that the velocity of the yarn relative to the air is identical to its velocity

relative to the inertial reference frame. The effect of air entrainment due to the beating action of the balloon is ignored. It is also assumed that the normalized air-drag coefficient p_0 is constant along the whole length of the yarn in the balloon, and that it takes on a value appropriate to the velocity of the yarn at the maximum balloon radius.

4.1 Air-drag coefficient

Fig. 7 shows the comparisons of the theoretical and experimental normalized curves of tension at guide-eye against yarn-length in balloon, where the experimental data came from the spinning experiments using cotton 38 tex (1 tex = 1 g/1,000 m) single yarn, cotton 50.4 tex and pure wool 70.1 tex two-fold yarns. The theoretical curve came from simulations with normalized air-drag coefficients. In order to estimate the value of p_0 to be used in simulating the motion of a particular yarn we ran the simulation for a range of values of p_0 and then plotted the simulated T_0 vs. s_l curves on top of the experimental curve. The value of p_0 used for the simulation that came closest to coinciding with the experimental curve in the neighbourhoods of the first few turning points was then used as the 'best fit' value of p_0 for that yarn. The normalized air-drag coefficient (p_0) equals 5.0 for 38 tex single cotton yarn, 4.0 for 50.4 tex two-fold cotton yarn and 3.3 for 70.1 tex two-fold wool yarn, respectively. We can use the same method to estimate the normalized air-drag coefficient for any yarn of specific type and count in ring spinning.

Using the relationship between C_D and p_0 described in section 2.1, we can calculate the air-drag coefficient (C_D). In particular, when the balloon-height is 0.3 m and ring radius is 0.03 m, the air-drag coefficients on the ballooning cotton single yarn, cotton and wool two-fold

yarns are displayed in Table 2. Furthermore, we can predict the air-drag on a ballooning yarn using Equation (1*c*).

4.2 Balloon shape and tension in a ballooning yarn

Figs 8(A_1) and 8(B_1) show the shapes of ballooning yarn with normalized air-drag coefficient (p_0) = 3.3 at a balloon-height of 10 for various yarn-length in balloon from simulations, whereas Figs 8(A_2) and 8(B_2) display the balloon shapes which were captured from the spinning experiments of pure wool 70.1 tex two-fold yarn [20]. Fig. 8(*C*) shows the locations corresponding to these balloon shapes in the curve of tension at guide-eye against yarn-length in balloon. Fig. 8 indicates that the experimental balloon shapes confirmed the results from simulations very well. Since the offset-angle in balloon is one of the outputs from simulation and the number of loops[†] in the balloon depends on the offset-angle, the balloon shape in ring spinning can be predicted based on the given yarn-length in balloon. Details of the data for one example from simulation can be found in Table 1.

Furthermore, the tension at guide-eye and balloon radius can be obtained from simulation for a selected yarn and given the yarn-length in balloon. Therefore we can estimate the tension in the ballooning yarn using Equation (3*d*).

4.3 The effect of yarn type and count on air-drag coefficient

[†] The yarn in the balloon follows a helical path with variable radius, and the surface of revolution generated by the rotating yarn is called a 'yarn balloon' in the textile industry. This is what the eye sees if the yarn loop is rotating at high speed in textile yarn machinery. The number of waves in the radius of the balloon is referred to here and elsewhere as the 'number of loops' in the balloon.

A yarn with specific type and linear density (or count) corresponds to a value of normalized air-drag coefficient on the ballooning yarn. Three examples are shown in Fig. 7. The data in Table 2 indicate that the value of normalized air-drag coefficient on a ballooning yarn is inversely proportional to the yarn diameter which is determined by the yarn type and yarn linear density. This agrees with previous result [21].

It should be pointed out that the effect of yarn hairiness on air-drag has not been considered to be a parameter in the above theoretical model. In fact, the air-drag on a ballooning yarn increases with an increase in yarn hairiness [22].

4.4 The effect of air-drag coefficient on yarn tension

Fig. 4 shows plots of normalized guide-eye tension versus normalized yarn length in the balloon for various values of the normalized air-drag coefficient. We note that when s_l is small (10.3) and when s_l is quite long (13.0) varying the air-drag has little effect on the guide-eye tensions. The main effect of varying p_0 is the variation in the locations of the turning points on T_0 vs. s_l curves.

Fig. 9 shows a 3-D plot of guide-eye tension versus s_l and p_0 and the changes in the locations of the turning points as air-drag increases are clearly seen. As the air-drag coefficient increases, the hysteresis fold in the tension surface slowly unfolds and finally disappears as the air-drag coefficient approaches 7.

4.5 The effects of balloon loops on yarn tension

When the yarn-length in balloon is close to the "minimum" value of $\sqrt{h^2 + a^2}$ (where h is the balloon-height and a is the ring radius), such as s_l = 10.05 for balloon-height of 10, the balloon is almost in the axial plane – the offset-angle is about 14°, which has one loop and the tension at guide-eye has the "maximum" value. When the yarn-length in balloon is increased, the balloon offset-angle increases due to the air-drag on the ballooning yarn and the balloon forms multiple loops. Within the same number of loops in the balloon, the tension keeps almost the same as the yarn-length in balloon varies throughout when the balloon has two or more loops. However, the tension at guide-eye decreases significantly while the balloon loops change from single to double and change from double and triple, as shown in Fig. 7. Further more, based on the experimental data (in the third, fifth and seventh columns, from left to right) in Table 3, we have

$$T_{n+1} = T_1/(n\pi) \qquad (n = 1 \rightarrow 3) \tag{5}$$

where T_1 is the average tension at guide-eye when the balloon has single loop, T_{n+1} is the average tension at guide-eye when the balloon has $(n + 1)$ loops $(n = 1 \rightarrow 3)$.

Table 3 shows the average tensions at guide-eye for various balloon loops. The theoretical results were confirmed by experimental data very well. The data in Table 3 indicate that it is a good method to reduce yarn tension by increasing loops in the balloon. The 'collapsed balloon spinning' has been used in practice for this reason.

4.6 The effect of balloon-height on yarn tension

In Fig. 10, the tensions at guide-eye are very close together for balloon-height (h) of 4, 5, …, 10, 11 and 12 when $s_l = 1.65h$. However, when $s_l = 1.02h$, the tensions at guide-eye increase

slowly as balloon-height varies from 4 to 10, but the tensions at guide-eye have a noticeable increase as balloon-height varies from 10 to 12. It suggests that normalized balloon-heights should not be greater than 10 in ring spinning.

Fig. 10 also shows that when balloon-height decreases, the number of hysteresis folds in the tension surface reduces, and there are fewer loops when balloon-height is shorter. Fig. 11 shows the results from theoretical model agree with the experimental data.

Fig. 12 displays a comparison of the tension at guide-eye for the given ratio of yarn-length in balloon to balloon-height from simulations at fixed p_0 = 4.0 and from the experiments of cotton 50.4 tex two-fold yarn. The results from both theory and experiments show that, when balloon-height varies from 4 to 12, the yarn tension slightly decreases if $s_l \geq 1.2h$, the yarn tension increases first and then decreases if $s_l = 1.1h$, and the yarn tension decreases first and then increases if $s_l \leq 1.03h$.

Fig. 12 indicates that the effect of the ratio of yarn-length in balloon to balloon-height is much larger than that of balloon-height itself.

5 Conclusion

A method of estimating the air drag coefficient p_0 that appears in the theoretical model of yarn balloon in ring spinning and predicting the tension in ballooning cotton and wool yarns was proposed. This method could be adopted in ring spinning mills to reduce yarn breakage and then to decrease energy consumption and increase yarn productivity. The results indicate that:

- The air-drag coefficient on a ballooning yarn is determined by the type and count of the yarn and then the air-drag on the ballooning yarn can be predicted using estimated air-drag coefficient.
- The balloon shapes can be simulated accurately. Therefore, balloon loops and tension in balloon can be predicted for specific yarn based on the simulation's outputs – the tension at guide-eye and offset-angle.
- Yarn tension increases when normalized balloon-height increases, particularly when the height is greater than 10. When the ratio of yarn-length in balloon to balloon-height is greater than 1.2, the yarn tension has a "lower" value and the effect of balloon-height on the tension is very weak.

6 Acknowledgment

This work was funded by a grant from the Australian Research Council (ARC) under its Discovery Project scheme. We would like to thank Dr. Lijing Wang and Mr. Chris Hurren at Deakin University for assisting with the experimental work.

References

[1] H. Stalder, Ring-spinning advance, *Textile Asia*, March 2000, 43–46.

[2] W. Klein, The technology of short-staple spinning (Short-staple spinning series), The Textile Institute Manual of Textile Technology, 1986, p. 51.

[3] G. M. Bracewell, K. Greenhalgh, Dynamical analysis of the spinning balloon, *J. Text. Inst.* **44** (1953) T266–T290.

[4] A. E. De Barr, A descriptive account of yarn tensions and balloon shapes in ring spinning, *J. Text. Inst*. **49** (1958) T58–T88.

[5] A. E. De Barr, The physics of yarn tensions and balloon shapes in spinning, winding and similar processes, *J. Text. Inst*. **51** (1960) T17–T38.

[6] A. E. De Barr, The role of air drag in ring spinning, *J. Text. Inst*. **52** (1961) T126–T139.

[7] S. K. Batra, T. K Ghosh, M. I. Zeidman, An integrated approach to dynamic analysis of the ring spinning process – part I: Without air drag and coriolis acceleration, *Textile Res. J.* **59**(6) (1989) 309-317.

[8] S. K. Batra, T. K Ghosh, M. I. Zeidman, An integrated approach to dynamic analysis of the ring spinning process – part II: With air Drag, *Textile Res. J.* **59**(7) (1989) 416–424.

[9] W. B. Fraser, On the theory of ring spinning, *Phil. Trans. R. Soc. Lond.* A, **342** (1993) 439–468.

[10] W. B. Fraser, The effect of yarn elasticity on an unwinding balloon, *J. Text. Inst*. **83**(4) (1992) 603–613.

[11] W. B. Fraser, Air drag and friction in the two-for-one twister: results from the theory, *J. Text. Inst.* **84**(3) (1993) 364–375.

[12] W. B. Fraser, L. Farnell, D. M. Stump, Effect of yarn non-uniformity on the stability of the ring-spinning balloon, *Proc. R. Soc. Lond.* A, **449** (1995) 597–621.

[13] J. D. Clark, W. B. Fraser, R. Sharma, C. D. Rahn, The dynamic response of a ballooning yarn: theory and experiment, *Proc. R. Soc. Lond.* A, **454** (1998) 2767–2789.

[14] F. Zhu, R. Sharma, C. D. Rahn, Vibrations of ballooning elastic strings", *J. Appl. Mech.* **64** (1997) 676–683.

[15] F. Zhu, K. Hall, C. D. Rahn, Steady state response and stability of ballooning strings in air, *Int. J. Non-linear Mechanics*, **33**(1) (1998) 33–46.

[16] R. Sharma, C. D. Rahn, An experimental study of ballooning yarn with a control ring, *J. Text. Inst*. **89**(4) (1998) 621–634.

[17] W. H. Press, B. P. Flannery, S. A. Teukolsky, W. T. Vetterling, *Numerical Recipes – The art of Scientific Computing*, Cambridge University Press, 1986, Chapter 16.

[18] The MathWorks, *MATLAB – The language of technical computing,* Version 6.5 , The MathWorks, Inc. 2003.

[19] Z. X. Tang, X. Wang, W. B. Fraser, L. Wang, An experimental investigation of yarn tension in simulated ring spinning, *Fibers and Polymers*, **5**(4) (2004) 275–279.

[20] Z. X. Tang, X. Wang, W. B. Fraser, L. Wang, Simulations of yarn winding in ring spinning, The 4th AUTEX Conference, 22–24, June 2004, Roubaix, France.

[21] J. D. Anderson, *Fundamentals of aerodynamics*, 3rd edition, McGraw-Hill, Inc. (2001).

[22] Z. X. Tang, X. Wang, W. B. Fraser, L. Wang, The effect of yarn hairiness on air drag in ring spinning, *Textile Res. J.* (In press).

Tables

Table 1. Tension at guide-eye, offset-angle and approximate error at varying yarn-length in balloon from simulation

Yarn-length in balloon (s_l) [normalized]	Tension at guide-eye (T_0) [normalized]	Radius tangent at guide-eye ($r'(0)$) [scalar]	$\|r(s_l) - 1\| + \|z(s_l) - H\|$ (E) [normalized]	Offset-angle[#] (φ) [radian]
10.05	33.9500	0.1700	0.0741	0.2479
10.30	15.7000	0.3000	0.0141	1.1811
10.50	5.3601	0.3400	0.0032	3.2905
11.00	3.6001	0.4075	0.0053	4.6386
11.50	2.0801	0.4400	0.0139	6.9843
12.00	1.9601	0.4625	0.0040	7.7135
12.50	1.8801	0.4775	0.0087	8.4103
13.00	1.6001	0.4875	0.0232	9.7475
13.50	1.5601	0.5000	0.0222	10.3983
14.00	1.5401	0.5075	0.0134	10.9014
14.50	1.5251	0.5150	0.0131	11.2564
15.00	1.5101	0.5225	0.0094	11.6110
15.50	1.4951	0.5275	0.0141	12.1192
16.00	1.4801	0.5325	0.0144	13.3568
16.50	1.4800	0.5375	0.0236	13.8643

[#] See section 2.3*b*.

Table 2. Modelling air-drag coefficient on ballooning cotton and wool yarns

Yarn type and count	m [kg/m]	p_0 [scalar]	C_D [scalar]
Cotton 38 tex single yarn	38×10^{-6}	5.0	2.98
Cotton 50.4 tex two-fold yarn	50.4×10^{-6}	4.0	1.94
Pure wool 70.1 tex two-fold yarn	70.1×10^{-6}	3.3	1.75

Table 3. Comparison of tension at guide-eye from experiments and prediction.

		Cotton 38 tex single yarn		Cotton 50.4 tex two-fold yarn		Pure wool 70.1 tex two-fold yarn	
		Experimental	Predicted	Experimental	Predicted	Experimental	Predicted
Average tension at guide-eye	1 loop	16.9357	16.9357	15.1167	15.1167	16.2006	16.2006
	2 loops	4.2813	5.3908	4.6892	4.8118	4.3133	5.1568
	3 loops	2.1658	2.6954	2.0456	2.4059	2.1453	2.5784
	4 loops	1.4937	1.7969	1.5198	1.6039	1.4400	1.7189
	5 loops	1.0650	1.3477	1.2179	1.2029	1.4117	1.2892

Captions to figures

Fig. 1. The ring spinning process.

Fig. 2. Schematic diagram of the experimental yarn balloon apparatus, where LS is a lead-screw, TS is a tension-measuring device, O is guide-eye, CM is a crank mechanism, DW is the drive wheel of the crank mechanism and DM is a drive motor [13].

Fig. 3. The cylindrical coordinates of a material point $\boldsymbol{P}$ on a ballooning yarn are r, θ, and z.

Fig. 4. The simulated curves of tension at guide-eye against yarn-length in balloon at balloon-height of 10 and for varying air-drag coefficients (All units are normalized).

Fig. 5. The lag angle of a ballooning yarn at the rotating eyelet relative to the plane containing the axis of rotation and the yarn tangent vector at the guide-eye.

Fig. 6. The experimental set-up for measuring yarn tension at the guide-eye: (*a*) Whole balloon testing device and (*b*) A close view of the measuring unit and the yarn guide.

Fig. 7. The curves of tension at guide-eye against yarn-length in balloon at balloon-height of 10 from simulations and from experiments (All units are normalized).

Fig. 8. The comparison of balloon shapes obtained from simulations ((A_1) s_l = 11.0 & (B_1) s_l = 13.5) and experiments ((A_2) & (B_2)) and the locations corresponding to these balloon shapes in the curve of tension at guide-eye against yarn-length in balloon (C).

Fig. 9. The predicted surface of tension at guide-eye on a ballooning yarn (h = 10).

Fig. 10. The simulated tension at guide-eye against yarn-length in balloon at fixed air-drag coefficients and for varying balloon-height (All units are normalized).

Fig. 11. The curves of tension at guide-eye against yarn-length in balloon between simulations at fixed air-drag coefficient of 4.0 and from experiments for cotton 50.4 tex two-fold yarn.

Fig. 12. The tension at guide-eye for the given ratio of yarn-length in balloon to balloon-height from simulations at fixed p_0 = 4.0 and from experiments for cotton 50.4 tex two-fold yarn.

Figures

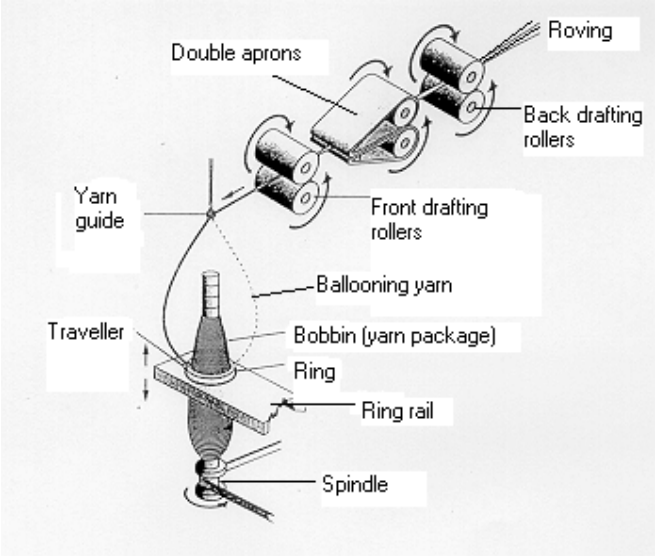

Fig. 1. The ring spinning process.

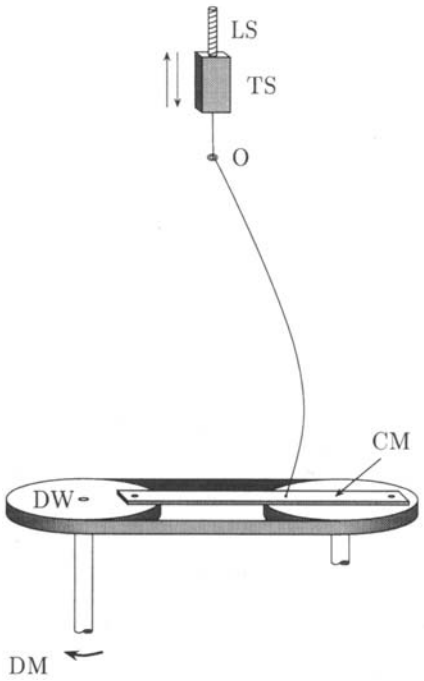

Fig. 2. Schematic diagram of the experimental yarn balloon apparatus, where LS is a lead-screw, TS is a tension-measuring device, O is guide-eye, CM is a crank mechanism, DW is the drive wheel of the crank mechanism and DM is a drive motor [13].

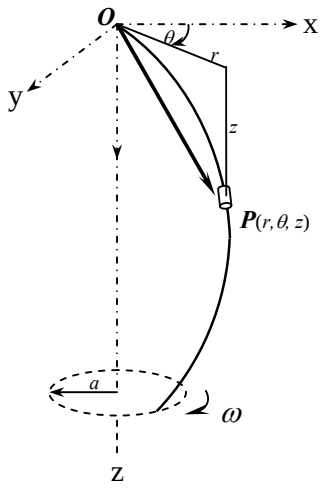

Fig. 3. The cylindrical coordinates of a material point ***P*** on a ballooning yarn are r, θ, and z.

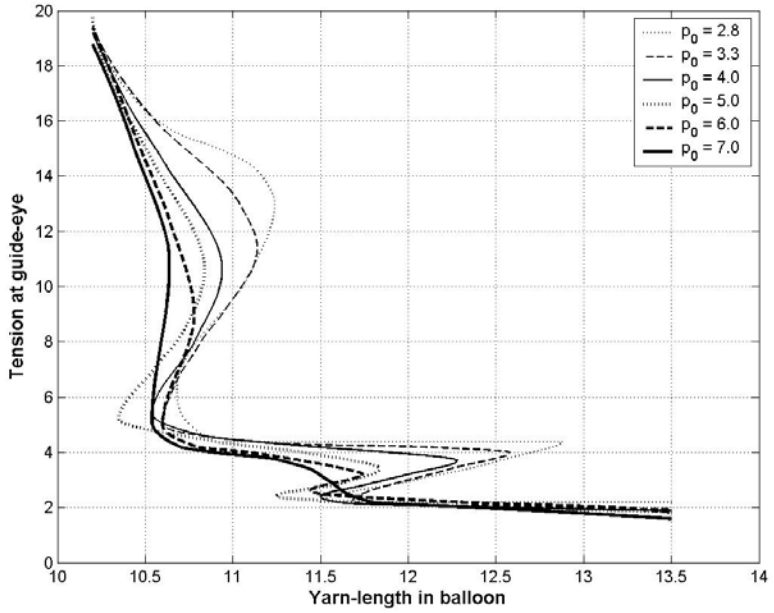

Fig. 4. The simulated curves of tension at guide-eye against yarn-length in balloon at balloon-height of 10 and for varying air-drag coefficients (All units are normalized).

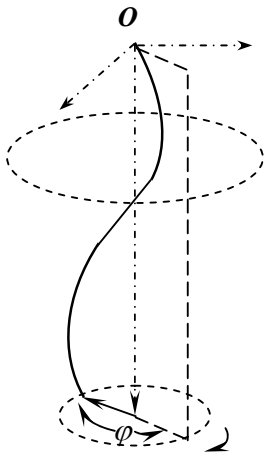

Fig. 5. The lag angle of a ballooning yarn at the rotating eyelet relative to the plane containing the axis of rotation and the yarn tangent vector at the guide-eye.

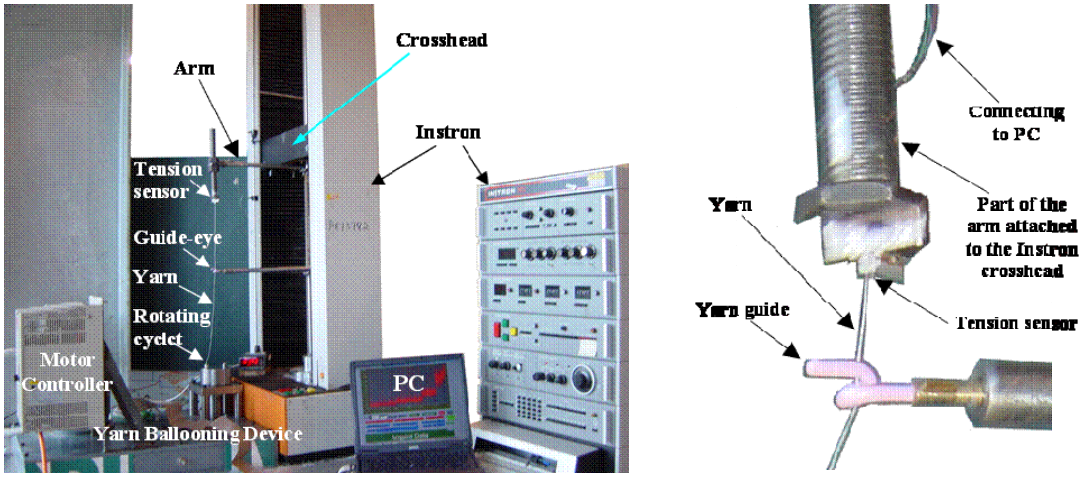

(*a*) (*b*)

Fig. 6. The experimental set-up for measuring yarn tension at the guide-eye: (*a*) Whole balloon testing device and (*b*) A close view of the measuring unit and the yarn guide.

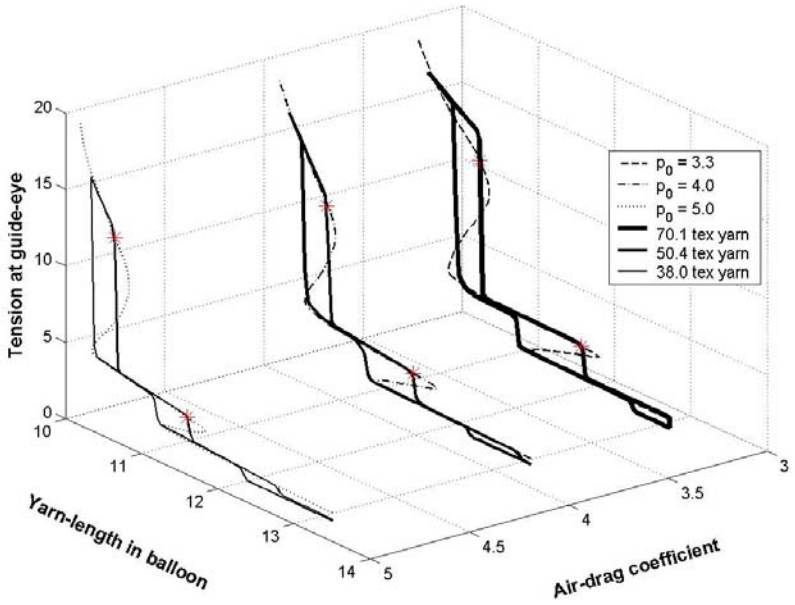

Fig. 7. The curves of tension at guide-eye against yarn-length in balloon at balloon-height of 10 from simulations and from experiments (All units are normalized).

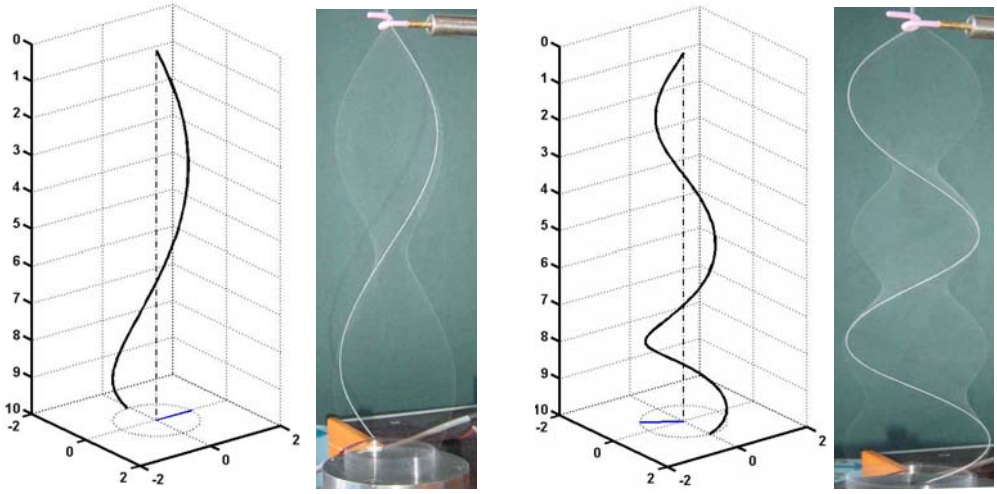

(A_1) (A_2) (B_1) (B_2)

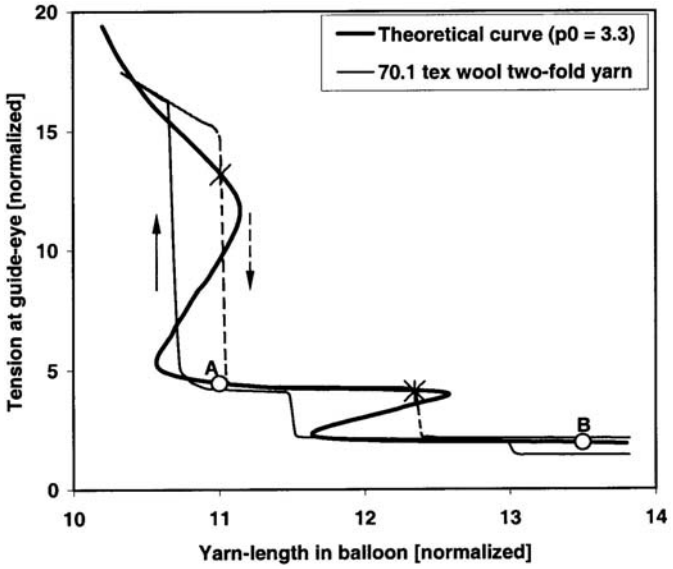

(C)

Fig. 8. The comparison of balloon shapes obtained from simulations ((A_1) s_l = 11.0 & (B_1) s_l = 13.5) and experiments ((A_2) & (B_2)) and the locations corresponding to these balloon shapes in the curve of tension at guide-eye against yarn-length in balloon (C).

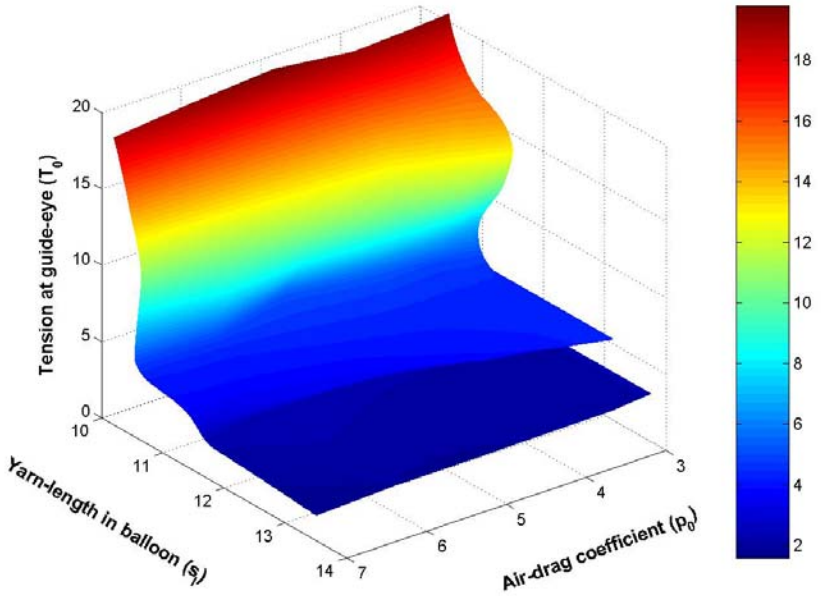

Fig. 9. The predicted surface of tension at guide-eye on a ballooning yarn (h = 10).

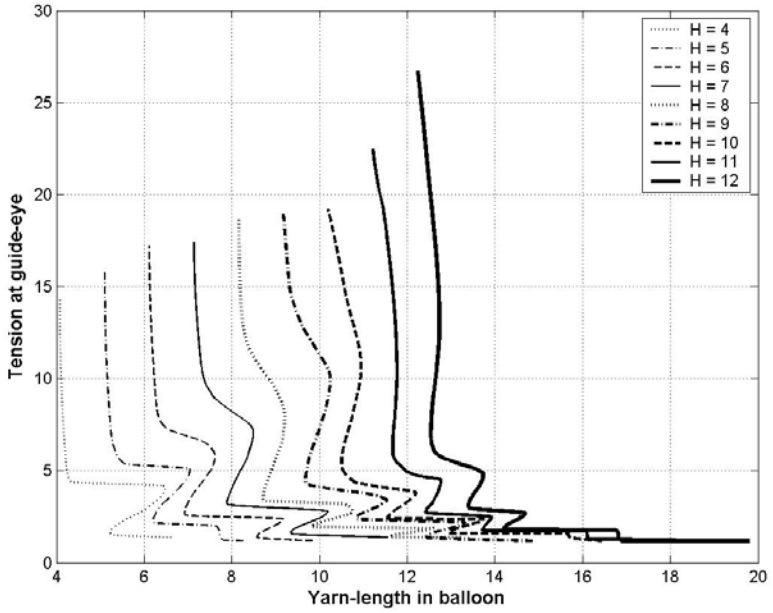

Fig. 10. The simulated tension at guide-eye against yarn-length in balloon at fixed air-drag coefficients and for varying balloon-height (All units are normalized).

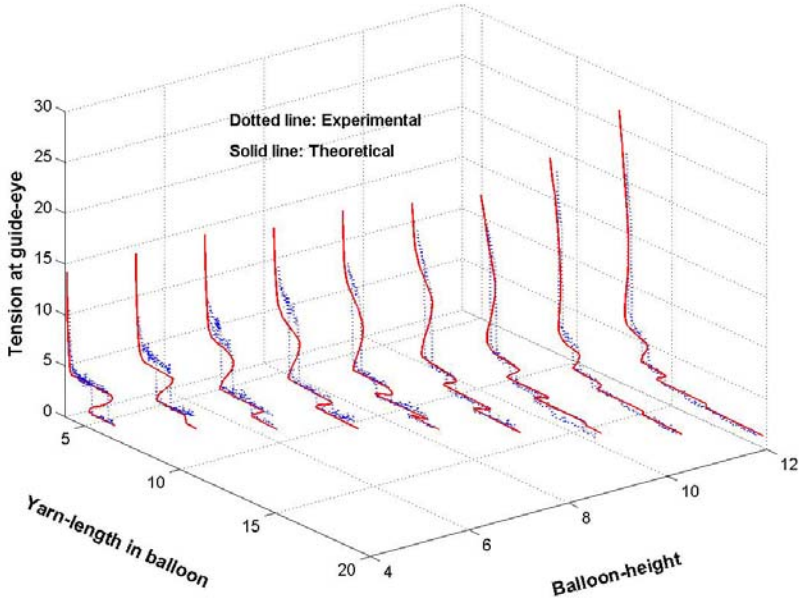

Fig. 11. The curves of tension at guide-eye against yarn-length in balloon between simulations at fixed air-drag coefficient of 4.0 and from experiments for cotton 50.4 tex two-fold yarn.

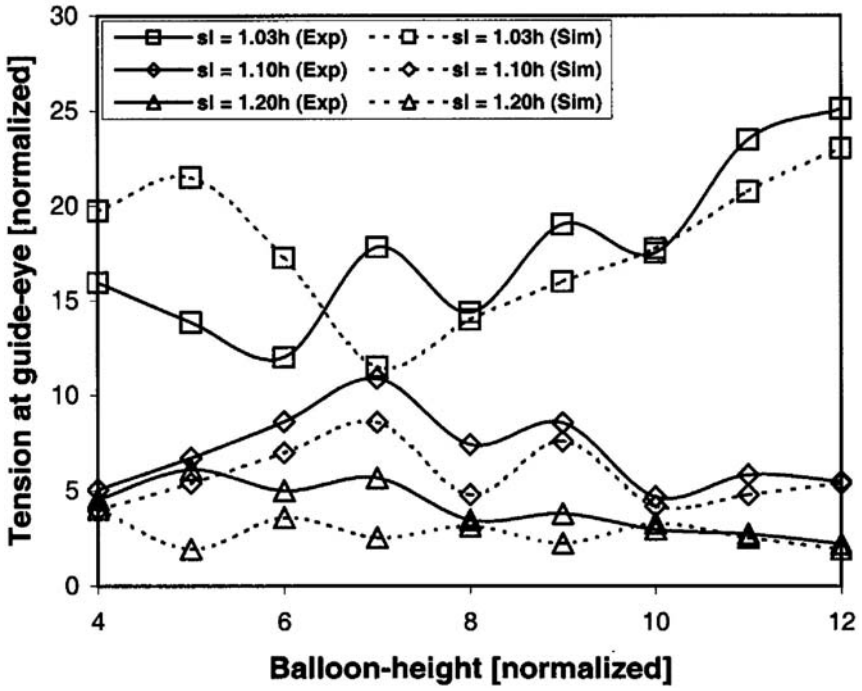

Fig. 12. The tension at guide-eye for the given ratio of yarn-length in balloon to balloon-height from simulations at fixed p_0 = 4.0 and from experiments for cotton 50.4 tex two-fold yarn.